Journal of Metals, Materials and Minerals, 35(1), e2274, 2025

Synergistic effects of $Ti_3C_2T_x$ MXene on the structural and dielectric properties of blend-based dielectrics

Nitesh Kumar NATH[1], Rajanikanta PARIDA[2], Bichitra Nanda PARIDA[3], and Nimai Charan NAYAK[1,*]

[1] *Micro and Nano Materials Laboratory, Department of Chemistry, Faculty of Engg &Technology (ITER), Siksha 'Anusandhan (Deemed to be University), Khandagiri Square, Bhubaneswar, Odisha-751030, India*

[2] *Department of physics, Faculty of Engg & Technology (ITER), Siksha 'O'Anusandhan (Deemed to be University), Khandagiri Square, Bhubaneswar, Odisha-751030, India*

[3] *Central Institute of Technology, Kokrajhar (Deemed to be University, MHRD, Govt. of India) BTAD, Assam-783370, India*

***Corresponding author e-mail**: nimainayak@soa.ac.in

Received date:
27 December 2024
Revised date:
4 January 2025
Accepted date:
7 January 2025

Keywords:
2D composite;
MXene;
Dielectrics;
Structural
Morphology

Abstract

The PVDF/PMMA-Ti_3C_2Tx MXene composite (PMC) films are processed via the solution casting method. The various phases (α, β) of PVDF have been identified through analysis using an X-ray diffractometer and Fourier transform infrared spectroscopy instruments. The maximum percentage β phase (%) obtained was 73.15%, which corresponds to a 10.0 wt% composite film. The structural analysis revealed that the $Ti_3C_2T_x$ nanoparticles are immiscibly distributed throughout the blend matrix, allowing the electrical conductivity and dielectric constant values to noticeably increase at constant frequency. The highest dielectric loss of 0.077 and the highest dielectric constant (ε_r) of 191.5 (at 100 Hz) were observed in the nanocomposites (NCs) film having 20 wt% $Ti_3C_2T_x$ MXene. The relative permittivity rises with increasing filler content because of high electrostatics and the interfacial polarization between the neat blend ($–CH_2–CF_2$ dipole) and filler. The percolation behavior is displayed by the conducting composite, and the percolation threshold has been shown to be more than 20 wt% MXene. The present study offers a novel perspective on the enhanced structural and dielectric properties of the composite system.

1. Introduction

The technique of combining two or more distinct polymer types to produce a new material having the combined qualities of the constituent polymers is known as polymer blending. The purpose of blending is frequently to combine the advantages of various polymers, such as increasing electrical, thermal stability, or to produce a material that is easier to process or more affordable. The miscibility of the blend determines the ultimate qualities, which are greatly influenced by the morphologies of the blend composite. The complimentary qualities of poly(methyl acrylate) (PMMA) and poly(vinylidene fluoride) (PVDF) blends receive a great attention [1]. PMMA provides stiffness, good impact strength, and optical clarity, whereas PVDF is renowned for its superior toughness, thermal stability, and chemical resistance. There are five distinct polymorphs of the semi-crystalline thermoplastic PVDF polymer, including α, β, γ, δ, and ε [2]. The non-polar α phase is the most common and stable and β, γ, and δ phases are electroactive. The β phases are mostly seen in different PVDF-based system due to its trans-planar zigzag structure. However, it is quite difficult to create electroactive phases using simple approaches. There are numerous studies in the literature on producing electroactive β phase by high voltage poling and uniaxial mechanical stretching at elevated temperatures [3-4]. Consequently, PVDF exhibits pyroelectric, ferroelectric, and piezoelectric activity upon the generation of electroactive phases. PMMA is a transparent amorphous polymer that is utilized in wide range of sectors, including display screens, acrylic glass (Plexiglas), and prostheses.

MXenes is a transition metal carbides/nitride, which garnered significant interest as a novel class of 2D materials. MXenes are created by selectively etching the A layers from MAX phases ($M_{n+1}AX_n$). The formula for MXene is $M_{n+1}X_nT_x$, where M is an early transition metal, and X is C or N and T_x is the surface termination group (–O, –OH, –F, etc.), respectively. MXenes are a promising material for a variety of applications like triboelectric nanogenerators (TENGs) and self-powered technologies due to their special qualities, which include outstanding flexibility, metallic conductivity, and great hydrophilicity [5-6]. The insulating polymers are incorporated with conducting fillers, like graphite [7], graphitic carbon nitride (g–C_3N_4) [8] and carbon nanotubes [9] to customize electrical conductivity. The electrical percolation threshold is the filler concentration at which electrical conductivity increases by several orders of magnitude. The electrical percolation threshold should be lowered as much as feasible to facilitate the production of conducting composites or blends. According to Martins *et al.* [10], PVDF-MWCNT composites have an electrical percolation threshold of 1.2 wt%. The impact of adding graphite nano-platelets to PVDF and PVDF/PMMA blends on electrical percolation and crystallization has been thoroughly examined by Chiu *et al.* [11]. The electrical resistivity of ternary composites is lower than that of

binary composites as per their findings. The literature has relatively few systematic investigations of the electrical properties, electroactive phase formation, and associated thermal characterizations of PVDF/PMMA blends including delaminated $Ti_3C_2T_x$ MXene. Therefore, the structural, morphological, thermal and electrical properties of the ternary composite are presented in this study, which begins with the synthesis of $Ti_3C_2T_x$ MXene.

2. Experimental

2.1 Materials

PMMA (MW is 9.6 × 104 g·mol^{-1}) and PVDF (MW of 5.5 × 104 g·mol^{-1}) were purchased from HI Media Laboratories Pvt. Ltd. We purchased 98.0% AR-grade Ti_3AlC_2 MAX phase from Beijing Forsman Scientific Co. Ltd. Qixian Huihongyuan Chemical Co. Ltd. (Shanxi, China) provided an aqueous HF solution (40.0%, AR grade). The N, N-dimethylformamide (DMF) and ethanol used to create composite sample was supplied by Macron Fine Chemicals.

2.2 Synthesis of $Ti_3C_2T_x$ MXene

First, 10 g of MAX powder were gradually added to 100 mL of a 40% concentrated HF solution, and the mixture was magnetically agitated at 40°C for 24 h. Deionized water and ethanol were used to repeatedly wash the resulting solution until the pH was between 4 to 5. To delaminate the resulting multilayered flakes of MXene powder, the synthesized MXenes and 60 mL of DMSO were magnetically agitated for 2 h at room temperature following washing. The resultant suspension was then centrifuged for 30 min at 9,000 rpm, washed with ethanol and dried in a vacuum oven at 60°C for 12 h.

2.3 Synthesis of PMC films

The required amount of PVDF and PMMA (2 g each) is first dissolved individually in 15 mL of N-N-dimethylacetamide at 60°C using a hot plate and a mechanical stirrer. Subsequently, the resultant PVDF/PMMA blend solution and the as-prepared MXenes solution were magnetically agitated (600 rpm) for 24 h. The mixture was sonicated for an hour in a water bath. The final residue was dried at 60°C for 10 h after being cast into a Petri dish with a diameter of 4 cm to 5 cm in a vacuum oven. The dry composite film was then molded (10 MPa pressure for 5 min) at 160°C in a flat vulcanization machine to create 1 mm thick sheets.

2.4 Characterization

An X-ray wavelength of 1.542 Å (Cu Kα radiation, 40 kV, 100 mA), a 2-theta diffraction angle of 5° to 80°, and a scanning rate of 10°·min^{-1} were employed to get the results of X-ray diffraction (XRD). A Carl Zeiss EVO-18 Field Emission Scanning Electron Microscope (FE-SEM) was used to analyze the surface texture. Fourier Transform Infrared Spectroscopy (FT-IR) was used to evaluate the samples using a Jasco FT-IR-4600 TYPE-A (wavelength range of 600 cm^{-1} to 4000 cm^{-1}). The dielectric properties and other electric functions were measured using an LCR meter (Model: PSM-1735, LCR N4L, UK) in the temperature range of 25°C to 100°C and the frequency range of 100 Hz to 5 MHz, respectively.

3. Results and discussion

3.1 Characteristics of $Ti_3C_2T_x$ MXene

The XRD patterns for Ti_3AlC_2 MAX powder and $Ti_3C_2T_x$ MXene are seen in Figure 1(a). The majority of the diffraction peaks vanished right away after HF etching in comparison to the pure Ti_3AlC_2 precursor, and the significant peak (002) shifted from 9.59° to 6.46°. This indicates that the Al layer from the precursor was successfully etched to create layered $Ti_3C_2T_x$. A small quantity of the original Ti_3AlC_2 MAX phase was found in MXene based on the XRD results. The conventional form of MXene is evident in the SEM image as seen in Figure 1(b), which displays a visible lamellar structure a few layers deep with a layered arrangement. The FESEM analysis shows that HF etching causes a gradual structural change of dense 2D layered structure to well-separated 2D layers of MXene nanosheets, which have a morphology similar to an "accordion"-like morphology [12]. The M-layers remain held together by weak Van der Waals bonds after the removal of the Al layers. The FTIR spectra of $Ti_3C_2T_x$ are displayed in Figure 1(c). The absorption peaks at 3446 cm^{-1} and 1506 cm^{-1} confirmed the presence of hydroxyl (–OH) groups and were attributed to the strongly hydrogen-bonded OH as well as the absorbed external water [13]. Furthermore, the peak at 620 cm^{-1} was most likely caused by the Ti-O bond, and the spectra of the two samples revealed the C–H (2921 cm^{-1}) and C–F (1095 cm^{-1}) groups.

3.2 Characteristics of composite thin film

3.2.1 XRD analysis

The structural modifications in the polymer caused by the processing technique used are illustrated in Figure 2. The solvent cast pure PVDF film displays peaks at 2θ positions of 18.5°, 20.3°, for α and β phase. There is also a broad peak at 38.8°, which are the typical monoclinic γ phase of PVDF as reported by Cai *et al.* [14]. However, the peak that correlated with the γ phase in our experiment remained unchanged when $Ti_3C_2T_x$ was added up to 10 wt%, and the broad peak disappeared at 39° due to increased filler loading. These results demonstrate that the γ phase of PVDF can transition to β phase as the peak corresponding to the γ phase broadens, depending on the loading of exfoliated MXene. However, the focus of four next studies will be on the compositional dependency of electroactive phase of PVDF. The filler particles in the produced composite have a high degree of crystallinity, as indicated by the sharp and strong peaks at $2\theta = 6.64°$. Using Scherrer's formula, the average crystallite size of the generated $Ti_3C_2T_x$ NPs was found to be 8.04 nm.

$$\text{Crystallite size (s)} = \frac{K\lambda}{\beta \cos\theta} \quad (1)$$

where β is the full width half maxima (FWHM), $\lambda = 0.154$ nm is the X-ray wavelength, K = 0.94 is the particle shape factor, and θ is Bragg's angle. However, it is seen that as the weight percentage of fillers increases, the intensities of the composite peaks rise linearly.

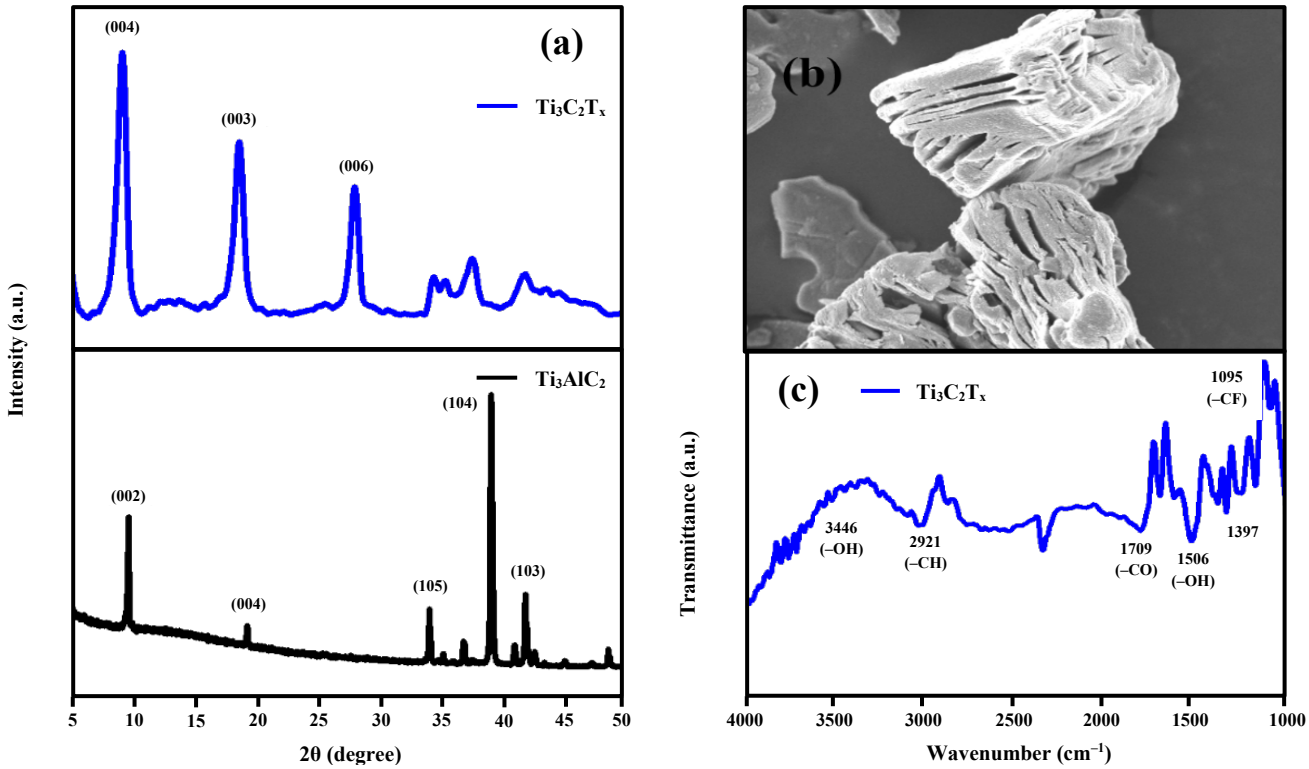

Figure 1. (a) XRD pattern of $Ti_3C_2T_x$ MXene, (b) FE-SEM images of $Ti_3C_2T_x$, and (c) The FT-IR spectra of $Ti_3C_2T_x$.

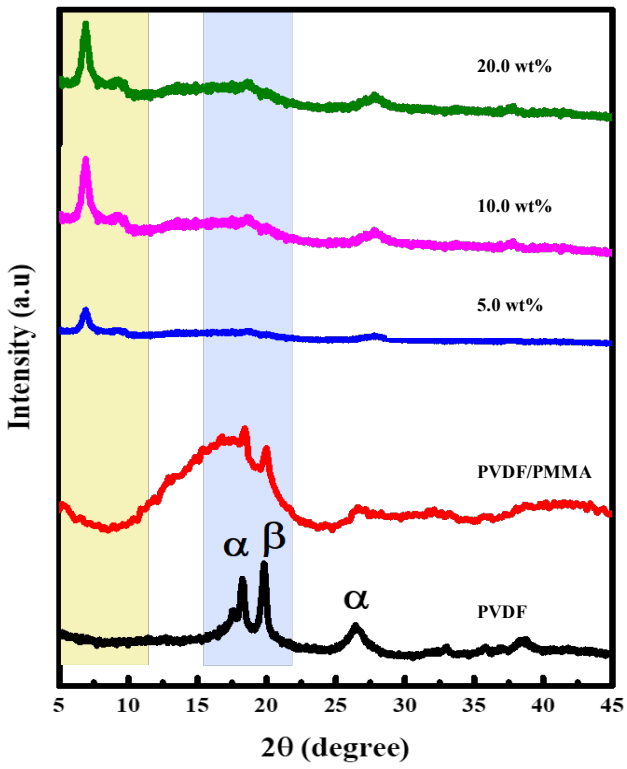

Figure 2. The XRD pattern of pure PVDF, neat blend and composite film.

3.2.2 Vibrational spectra

Figure 3(a). shows the results of an FTIR spectra of pure PVDF film, the PVDF/PMMA blend and composite varying concentrations of filler. The results show that, the addition of MXene does not change the phase of PVDF as indicated in XRD analysis. It has been observed previously that the distinctive bands at 834 cm^{-1} and 1233 cm^{-1} validate the electroactive β phase in the neat blend [14]. The α and γ phase of PVDF is associated to the other bands. It is important to note that the ferroelectric β-phase must predominate over the on-polar α-phase when constructing composites with PVDF. The percentage of β-phase (F_β) of PVDF can be determined using the following equation, which is provided by Gregorio and Cetari [15],

$$F_\beta = \frac{A_\beta}{1.26 \times (A_\alpha + A_\beta)} \quad (2)$$

The absorption coefficients for the α phase (762 cm^{-1}) and β phase (840 cm^{-1}) are denoted by Aα and A_β, respectively. Figure 3(b). shows a graphic representation of the percentage of the β phase vs the weight percentage of filler in the blend. The maximum β phase percentage obtained was 73.1% among all these composites. As a result, the XRD results are further validated by FTIR analysis.

3.2.3 Morphology analysis

The effect of $Ti_3C_2T_x$ NPs on the microstructure of the PMC films were investigated by FE-SEM analysis, as shown in Figure 4. The morphology of neat PVDF/PMMA blend is shown in Figure 4(a). The prepared nanocomposites showed very low MXene aggregation, according to Figure 4(b). The disintegration of acid molecules trapped between the layers of MXene plane causes the volume to rise. This eventually causes the planes to enlarge farther along the all-direction of the nanofiller, creating a porous structure. As a result, the MXene nanosheets maintains the efficient insulation by filling the gaps left by the blend matrix.

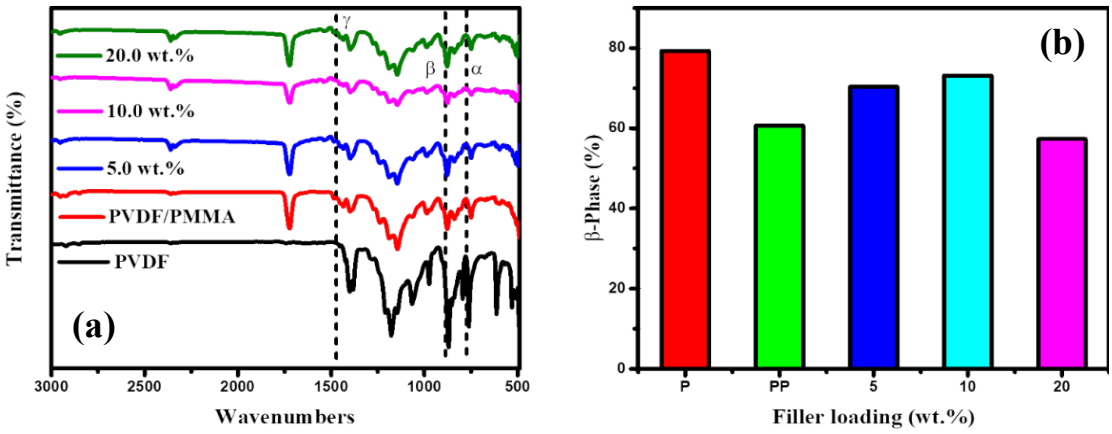

Figure 3. (a) FTIR spectra of polymer blend NCs with different concentrations of MXene, and (b) Fraction of the β phase from FT-IR data.

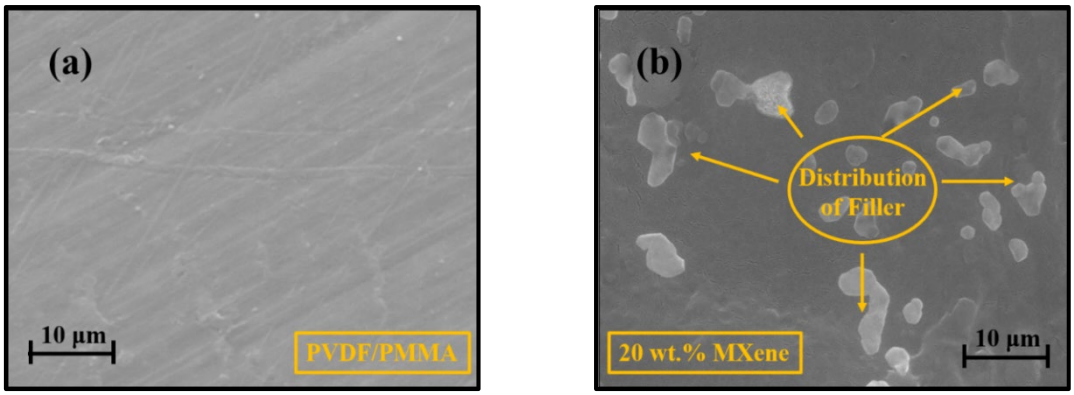

Figure 4. FE-SEM images of (a) pure PVDF/PMMA blend, and (b) PVDF/PMMA-20 wt% $Ti_3C_2T_x$ composite film.

3.2.4 Dielectric analysis

The frequency dependence of the relative permittivity (έ) and tangent loss (tan δ) of composite films are shown in Figure 5(a-b). The capacitance was measured at room temperature between 100 Hz and 1 MHz as a function of frequency. The dielectric parameter has been calculated using the well-known equations,

$$\varepsilon' = \frac{l \times C_p}{A \times \varepsilon_o} \tag{3}$$

where C_p is the parallel capacitance, ε_o is the permittivity of empty space, A is area and l are thickness of films, respectively. Initially, the permittivity of composite falls with increasing frequency due to the dipolar contribution being reduced at high frequencies (lag dipolar reversal). The main reason of the increase in permittivity when the filler content rises at a steady rate is the addition of $Ti_3C_2T_x$ MXene to the blend matrix, which has a greater conductivity. The permittivity rises uniformly from 7.18 (pure PVDF/PMMA) to 101 when 5 wt% of $Ti_3C_2T_x$ is added to the blend, and ε_r increases steadily from 101 to 191 when 20 wt% loading is added. It is possible to conclude that the percolation threshold is between 20 wt% and 25 wt%. The percolation threshold can be found using the method below,

$$\varepsilon' \propto (f_c - f)^s \text{ for } f < f_c \tag{4}$$

where s is the critical exponent related to characteristics of the material, f_c is the percolation threshold, and f is the volume fraction of filler concentration. The plot shows that f_c is 12.59 vol% (about 21.5 wt%), and 's' is 0.25 was found by fitting log έ vs log ($f_c - f$) linearly in Figure 5(c). The variation of the dielectric loss tangent at room temperatures with respect to frequency are shown similar trend, as seen in Figure 5(b). At lower frequency ranges, tangent loss first decreases and subsequently increases as filler content rises. The 10 wt% PMC film with tan δ value of 0.077 at 25°C at 100 Hz showed a significant increase in the loss tangent value. It may be caused by (i) interfacial polarization (Maxwell–Wagner–Sillars polarization) (ii) conduction loss brought on by the development of PVDF chains known as Debye kind of relaxation process [16]. In general, Maxwell-Wagner-Sillars polarization occurs because charges accumulate at the interfaces between regions with varying electrical conductivities and relative permittivity. The presence of –OH groups frequently leads to increased hydrophilicity and improved interaction with adsorbed water, which can raise conductivity and encourage MWS polarization. The high electronegativity of –F groups are able to localize charges more successfully, which leads to a distinct charge separation. Stronger ionic and covalent bonds are facilitated by –O groups, and depending on the local environment, these bonds can have varying effects on polarization dynamics [17]. Charge carriers have the ability to tunnel through thin insulating barriers at the nanoscale. Additional polarization channels are produced by this tunneling, which helps to increase in dielectric increase that is not explained by traditional percolation theory.

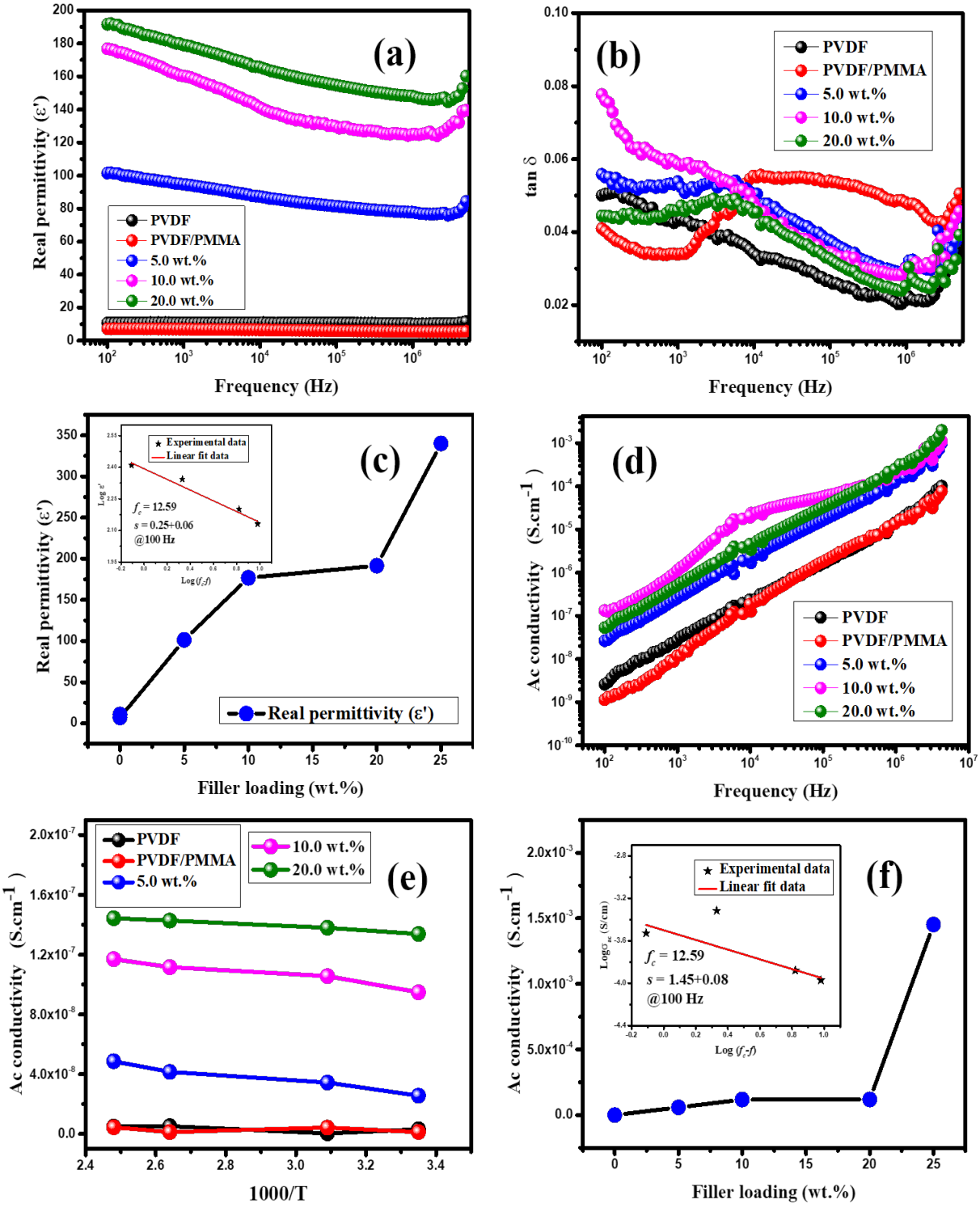

Figure 5. Frequency dependence of (a) real permittivity, (b) tan δ, (c) ε' of composites at 100 Hz with filler concentration, (d) AC conductivity, (e) AC conductivity vs 1000/T, and (f) AC conductivity of NCs with varying filler loading.

3.2.5 Conductivity analysis

The frequency dependence of the AC conductivity (σ_{ac}) in Figure 5(d). can be described using the Jonscher's power law equation ($\sigma_{ac} = \sigma(0) + A\omega^s$), where $\sigma(0)$ is the frequency independent part, also known as DC conductivity, and ω is the analogous frequency of the AC field in the frequency sensitive section [18]. The Maxwell-Wagner mechanism may be the primary cause of the conductivity rise, which is consistent with the low temperature and high frequency. The conductivities of the 20 wt% composite rise from 2.5×10^{-8} S.cm^{-1} to 3.2×10^{-4} S.cm^{-1} at 100 Hz and 1 MHz, respectively. Due to the formation of electrically conductive channels, conductivity and dielectric losses both increase with filler concentration. The bulk conductivity of the material is determined by fitting the AC conductivity plot with Jonscher's power law, indicating an electronic-transport mechanism within the sample, as shown in Figure 5(e).

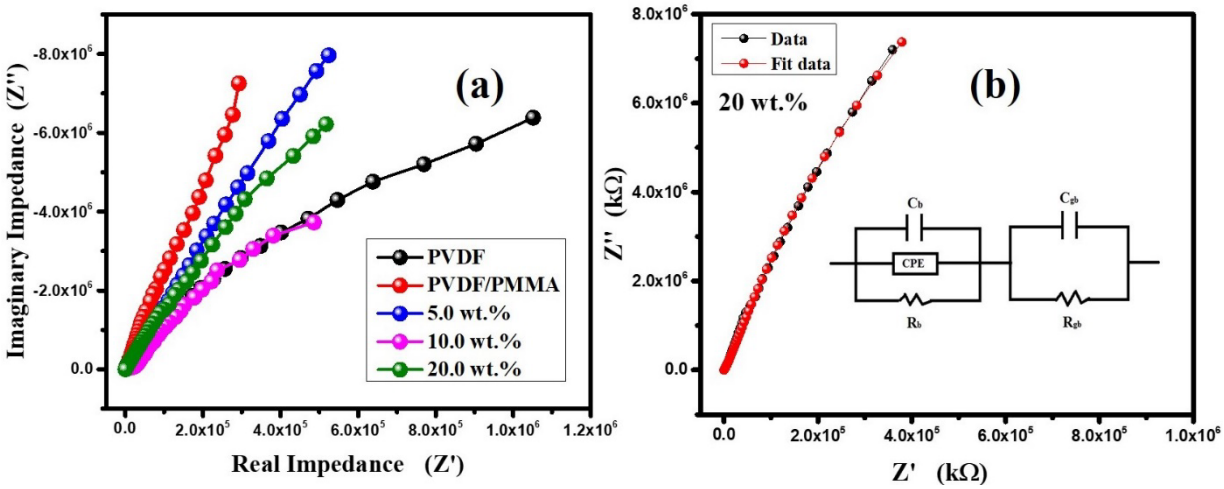

Figure 6. (a) Nyquist plot of the PVDF/PMMA blend composite with varying $Ti_3C_2T_x$ MXene, and (b) Circuit parameter employed in the fitting.

The conductivity of the composites below the percolation threshold can be predicted using the power law that follows,

$$\sigma \propto (f_c - f)^s \text{ for } f < f_c \quad (5)$$

where σ represents the conductivity, f represents filler concentration, and 's' represents the critical exponent. The plots show that the percolation thresholds (f_c) and 's' are 12.59 vol% and 1.45 measured at 100 Hz, respectively, based on the best fits of the experimental results in Figure 5(f). Conductive fillers start to cluster at concentrations close to f_c. The degree to which electrons or charge carriers can hop or tunnel between nearby fillers depends on the size and connection of these clusters. It is the spatial dimensions of the system that affect the value of critical exponent (s). It is easier for percolation routes to emerge in lower dimensionality materials (such as thin films), which leads to reduced "s" values. A more abrupt increase in conductivity occurs when fillers come into direct contact with one another. Systems that have a very homogeneous filler distribution may show a sharper transition (lower s value) [19].

3.2.6 Impedance analysis

The Nyquist plot (also known as a complex impedance) of the composite at room temperatures over a broad frequency range (100 Hz to 1 MHz) are displayed in Figure 6. The number of semicircles in a plot is commonly used to indicate the relaxation processes of a composite system. The characteristic frequency is the cut-off frequency at which composites change from resistive to capacitive behavior. In the case of all composite samples, there are not absolute circles but rather a diminished or enhanced semi-circle appearance in Figure 6(a). There may be a non-uniform distribution of filler in the NCs since these Nyquist plots are not continuous.

The Nyquist plots of the electrical circuit with the fitting parameters (R_g = grain resistance, C_g = grain capacitance, and CPE = constant phase element) are shown in Figure 6(b). It is experimentally demonstrated by fitting the experimental data that the phase element and depressed semicircular arcs with centers below the real Z' axis is confirmed that the relaxation process in the material is Non-Debye type. This indicates that the relaxation processes are improved by the $Ti_3C_2T_x$. It is important to note that the arcs that resemble semicircles in our cases are not complete because the equipment features restrict the frequency range of our tests.

4. Conclusion

The flexible and free-standing PVDF/PMMA blend composite films with $Ti_3C_2T_x$ have been processed through solution casting process. The presence of the polymer phases α and β was verified by XRD and FTIR, which also examined a variety of vibrational band transitions in the polymorphous PVDF. It has been demonstrated that adding the filler significantly increases the dielectric constant, making it almost 28 times higher than that of the pure blend film. At 1 MHz, a notable increase in conductivity to 3.2×10^{-4} S.cm^{-1} for 20 wt% film is seen. The semicircle shape Nyquist plot indicates the presence of extremely small relaxation processes. These composites have a lot of potential for use in storage and microwave absorption devices due to their significant increase in dielectric permittivity and extremely low loss tangents.

Acknowledgements

The authors are thankful of Dr. Bichitra Nanada Parida of Central Institute of Technology, Kokrajhar for performing Dielectric analysis.

Reference

[1] N. K. Nath, R. R. Mohanta, R. K. Parida, B. N. Parida, and N. C. Nayak, "Improving the energy storage efficiency and power density of polymer blend in combination with $Ti_3C_2T_x$ for energy storage devices," *Materials Today Chemistry*, vol. 41, p. 102338, 2024.

[2] V. O. C. Concha, L. Timoteo, L. A. N. Duarte, J. O. Bahu, F. Lopez, A. P. Silva, L. Lodi, P. Severino, J. I. Pulido, and E. B. Souto, "Properties, characterization and biomedical applications of polyvinylidene fluoride (PVDF): A review," *Journal of Materials Science*, vol. 59, no. 31, pp. 14185-14204, 2024.

[3] G. H. Kim, S. M. Hong, and Y. Seo, "Piezoelectric properties of poly (vinylidene fluoride) and carbon nanotube blends: β-phase development," *Physical Chemistry Chemical Physics*, vol. 11, no. 44, p. 10506, 2009.

[4] V. R. P, D. V. Khakhar, and A. Misra, "Studies on α to β phase transformations in mechanically deformed PVDF films," *Journal of Applied Polymer Science*, vol. 117, no. 6, pp. 3491-3497, 2010.

[5] S. He, Q. Zhu, R. A. Soomro, and B. Xu, "MXene derivatives for energy storage applications," *Sustainable Energy & Fuels*, vol. 4, no. 10, pp. 4988-5004, 2020.

[6] J. A. A. L. Jayarathna, S. Hajra, S. Panda, E. Chamanehpour, I. Sulania, M. S. Goyat, S.-H. Hsu, H. J. Kim, T. Treeratanaphitak, and Y. K. Mishra, "Exploring potential of MXenes in smart sensing and energy harvesting," *Materials Letters*, vol. 363, p. 136252, 2024.

[7] F.-C. Chiu, and Y.-J. Chen, "Evaluation of thermal, mechanical, and electrical properties of PVDF/GNP binary and PVDF/PMMA/GNP ternary nanocomposites," *Composites Part a Applied Science and Manufacturing*, vol. 68, pp. 62-71, 2014.

[8] M. P. Niharika, R. Garlapallya, K. Ruthvik, M. Velaga, and B. M. Rao, "Hydrogen production on g-C_3N_4 nanoflakes via photo-electrochemical water splitting," *Materials Today Proceedings*, 2023.

[9] K. Y. Fang, F. Fang, S. W. Wang, W. Yang, W. Sun, and J. F. Li, "Hybridizing CNT/PMMA/PVDF towards high-performance piezoelectric nanofibers," *Journal of Physics D Applied Physics*, vol. 51, no. 26, p. 265305, 2018.

[10] V. Khade, and M. Wuppulluri, "Microwave absorption performance of flexible porous PVDF-MWCNT foam in the X-band frequency range," *ACS Omega*, vol. 9, no. 33, pp. 35364-35373, 2024.

[11] N. Augustin, P. Muraliharan, A. Sabu, K. K. Senthilkumar, P. K. Annamalai, and R. B. T. S. Raghava, "Unravelling the role of poly(methyl methacrylate) (PMMA) molecular weight in poly(vinylidene fluoride) (PVDF)/PMMA/expanded graphite (ExGr) blend nanocomposites: Insights into morphology, thermal behavior, electrical conductivity, and wetting property," *Journal of Thermoplastic Composite Materials*, vol. 37, no. 8, pp. 2527-2570, 2024.

[12] P. R. Sumbe, U. Chhote, G. Sanyal, B. Chakraborty, A. Sayeed, and M. A. More, "Synthesis, physico-chemical characterization, DFT simulation, and field electron behaviour of 2D layered $Ti_3C_2T_x$ MXene nanosheets," *Nano Express*, vol. 5, no. 3, p. 035005, 2024.

[13] Y. Li, X. Zhou, J. Wang, Q. Deng, M. Li, S. Du, Y.-H. Han, J. Lee, and Q. Huang, "Facile preparation of in situ coated $Ti_3C_2T_x/Ni_{0.5}Zn_{0.5}Fe_2O_4$ composites and their electromagnetic performance," *RSC Advances*, vol. 7, no. 40, pp. 24698-24708, 2017.

[14] X. Cai, T. Lei, D. Sun, and L. Lin, "A critical analysis of the α, β and γ phases in poly (vinylidene fluoride) using FTIR," *RSC Advances*, vol. 7, no. 25, pp. 15382-15389, 2017.

[15] V. R. Jeedi, E. L. Narsaiah, M. Yalla, R. Swarnalatha, S. N. Reddy, and A. S. Chary, "Structural and electrical studies of PMMA and PVDF based blend polymer electrolyte," *SN Applied Sciences*, vol. 2, no. 12, 2020.

[16] N. K. Nath, R. R. Mohanta, R. K. Parida, B. N. Parida, and N. C. Nayak, "Structural, morphological, and dielectric properties of poly(vinylidene fluoride)/$(Bi_{0.5}Ba_{0.25}Sr_{0.25})(La_{0.5}Ti_{0.5})O_3$ composites," *Journal of Applied Polymer Science*, vol. 141, no. 31, 2024.

[17] M. Samet, V. Levchenko, G. Boiteux, G. Seytre, A. Kallel, and A. Serghei, "Electrode polarization vs. Maxwell-Wagner-Sillars interfacial polarization in dielectric spectra of materials: Characteristic frequencies and scaling laws," *The Journal of Chemical Physics*, vol. 142, no. 19, 2015.

[18] B. M. Greenhoe, M. K. Hassan, J. S. Wiggins, and K. A. Mauritz, "Universal power law behavior of the AC conductivity versus frequency of agglomerate morphologies in conductive carbon nanotube-reinforced epoxy networks," *Journal of Polymer Science Part B Polymer Physics*, vol. 54, no. 19, pp. 1918-1923, 2016.

[19] S. Tu, Q. Jiang, X. Zhang, and H. N. Alshareef, "Large dielectric constant enhancement in MXene percolative polymer composites," *ACS Nano*, vol. 12, no. 4, pp. 3369-3377, 2018.